JCTC Journal of Chemical Theory and Computation

Theoretical Study of the Magnetic Properties of an Mn_{12} Single-Molecule Magnet with a Loop Structure: The Role of the Next-Nearest Neighbor Interactions†

Joan Cano,§ Ruben Costa,‡ Santiago Alvarez,‡ and Eliseo Ruiz*,‡

Departament de Química Inorgànica and Centre de Recerca en Química Teòrica, Universitat de Barcelona, Martí i Franquès 1-11, 08028 Spain, and Institució Catalana de Recerca i Estudis Avançats (ICREA)

Received January 12, 2007

Abstract: The magnetic properties of a Mn_{12} single-molecule magnet with a loop structure are characterized by a computational study based on density functional theory. A study of the two reported crystal structures of such a complex correctly reproduces the experimental spin ground state. We have analyzed the effect of the choice of spin configurations employed for the calculations, as well as the influence of the inclusion of the next-nearest neighbor interactions on the calculated exchange coupling constants. Quantum Monte Carlo simulations performed with the calculated exchange coupling constants show that the best agreement with the experimental susceptibility curve is achieved by using the hybrid B3LYP functional.

Introduction

The synthesis and study of magnetic properties of large polynuclear transition metal clusters is a field to which many research groups have devoted considerable effort during the past years.[1] Some of those polynuclear complexes show a slow relaxation of the magnetization that could eventually lead to applications for information storage at the molecular level.[2,3] The first single-molecule magnet (SMM) reported was the $[Mn_{12}O_{12}(CH_3COO)_{16}(H_2O)_4]$ complex, usually know as Mn_{12} or Mn_{12} acetate, that adopts a compact cluster structure with a central cubane of four Mn^{IV} cations surrounded by a crown of eight Mn^{III} cations.[4] In order to have a slow relaxation of the magnetization, one needs a high-energy barrier between the states with positive and negative magnetic moments, and also quantum tunneling effects should be avoided.[5,6] Such a barrier is known to depend directly on the square of the total spin of the molecule and on its magnetic anisotropy parameter D, that in the case of the Mn_{12} acetate are $S = 10$ and $D = -0.46$ cm^{-1}.[7,8] Hence, high-spin and large, negative anisotropy-parameter polynuclear complexes are much sought after synthetic targets due to their possible technological applications.

In order to quantify the S value of the ground state for a polynuclear complex, we should employ a Heisenberg spin Hamiltonian that can be expressed as

$$\hat{H} = -\sum_{i>j} J_{ij}\hat{S}_i\hat{S}_j + D\left(\hat{S}_z^{\,2} - \frac{1}{3}\hat{S}^2\right) + E(\hat{S}_x^{\,2} - \hat{S}_y^{\,2}) \quad (1)$$

where $\hat{S}_i$ and $\hat{S}_j$ are the spin operators of paramagnetic centers i and j and $\hat{S}$ and $\hat{S}_z$ are the total spin operator of the molecule and its axial component, respectively. The J_{ij} values are the exchange coupling constants for the different pairwise interactions between the paramagnetic centers of the molecule, while D and E are the axial and rhombic components of the anisotropy, respectively. Spin-orbit coupling effects must be taken into account for the calculation of the zero-field splitting parameters D and E;[9−13] otherwise, only the exchange coupling constants can be determined. However, the study of the magnetic properties of such systems from magnetic susceptibility curves presents considerable problems from the experimental point of view due to the large number of states involved. For instance, a Mn_{12} complex containing six Mn^{II} and six Mn^{III} ions has 7.29×10^8 M_s states. For

† Dedicated to Professor Dennis R. Salahub on the occasion of his 60th birthday.

* Corresponding author e-mail: eliseo.ruiz@qi.ub.es.

‡ Universitat de Barcelona.

§ ICREA.

10.1021/ct700013g CCC: $37.00
Published on Web 04/21/2007

such a large number of states, even if symmetry is taken into account, it is impossible to build up the Hamiltonian matrix using a Heisenberg Hamiltonian (eq 1), as required to perform a fitting of the J values, due to the huge amount of memory required. Even in the case that the memory was available and it was possible to diagonalize the matrix, there are many sets of exchange coupling constants that may perfectly fit the experimental data. Thus, from only the experimental magnetic susceptibility data, it is possible to extract the total spin value of the ground state, whereas in inelastic neutron scattering experiments, one obtains the relative energies and spin values of the excited states.[14]

On the other hand, theoretical methods based on density functional theory have been employed to analyze the spin states. For instance, we can mention earlier studies devoted to simple molecules[15] and polynuclear metal clusters,[16] but it is only in recent years that each approach has been extensively employed. Such methodology also allows one to obtain all the exchange coupling constants present in polynuclear transition-metal complexes, information that is extremely useful for the future design of new molecular systems with improved magnetic properties.[13,17−20] For instance, the exchange interactions of the widely experimentally studied Mn_{12} acetate complex have been calculated using theoretical methods based on density functional theory by different authors.[13,21−24] In order to calculate the n J_{ij} exchange coupling constants of a polynuclear complex, we must at least perform $n + 1$ energy calculations of different spin configurations that correspond to single-determinant Kohn−Sham solutions.[25−27] Such spin configurations must be selected in a such way as to make it possible to solve a system of n equations with n unknowns, the J_{ij} values. However, some questions emerge at this point concerning the choice of a few spin configurations for the calculations among thousands of possibilities. Thus, an interesting point is to evaluate the dependence of the calculated J values on the selected set of spin configurations. This problem is directly related with the accuracy of the phenomenological Heisenberg Hamiltonian to describe the magnetic properties in such systems. In principle, if the exchange interactions can be properly described by the Heisenberg Hamiltonian, the calculated J values should be independent of the spin configurations selected. However, different authors have pointed out this problem, and it is usually proposed to calculate more energies than strictly needed and then perform a least-squares fitting to extract the exchange coupling constants until the calculated values converge.[13,28] Even if we can obtain a set of J values that remain unchanged upon increasing the number of spin configurations, there is still the problem of whether the simple Heisenberg Hamiltonian describes correctly such systems or we need to include some additional terms. In order to solve the limitations of the Heisenberg Hamiltonian employed, some approaches have been adopted, such as the inclusion of the often neglected next-nearest neighbor interactions or to include new three- or four-body spin terms in the Hamiltonian.[29] Theoretical methods can be employed to elucidate the importance of such terms. However, from the experimental point of view, it is a difficult task because of an increased number of fitting parameters, making it harder to obtain a unique fit.

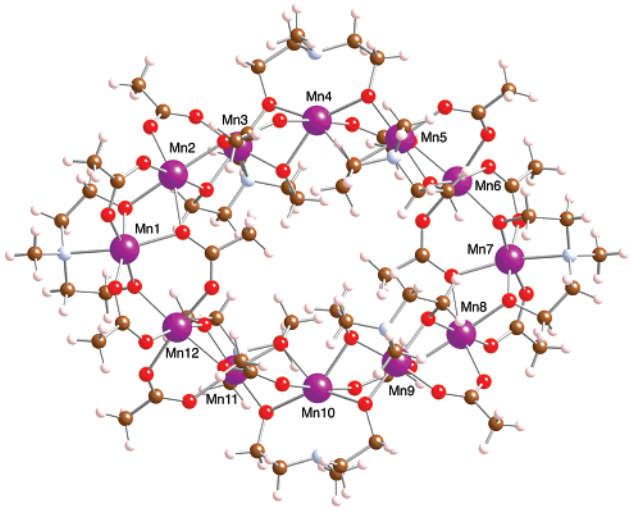

Figure 1. Molecular structure of the Mn_{12} complex, $[Mn^{III}_6Mn^{II}_6(O_2CMe)_{14}(mda)_8]$ ($mdaH_2$ = N-methyldiethanolamine).[30,31] Mn^{III} and Mn^{II} cations correspond to odd and even numbers, respectively.

The main goal of this work is to study the magnetic properties of a Mn_{12} complex with a loop structure (see Figure 1) showing SMM behavior. We have selected this system instead of other SMMs, such as, the first SMM Mn_{12} complex,[4] because its cyclic structure makes this system well-suited for an analysis of the role of the next-nearest neighbor interactions. This Mn_{12} compound was independently reported recently by Rumberger et al.[30,31] and Foguet-Albiol et al.[32] with two very similar crystal structures that show an alternation of Mn^{III} and Mn^{II} cations (see Figure 1). Even if the experimental susceptibility curves are relatively similar, the two groups have proposed different magnetic parameters for the ground state, $S = 8$ and $D = -0.47$ cm^{-1} and $S = 7$ and $D = -0.26$ cm^{-1}, respectively.

Results and Discussion

Magnetic Properties of the Mn_{12} Complex. We start our study of the magnetic properties of the Mn_{12} complex by calculating the exchange coupling constants while neglecting next-nearest neighbor interactions. The analysis of the geometry indicates the presence of six different exchange interactions. Thus, the topology of the interactions is represented in Figure 2, and the Heisenberg Hamiltonian has the following expression:

$$\begin{aligned}\hat{H} = &-J_1[\hat{S}_1\hat{S}_2 + \hat{S}_7\hat{S}_8] - J_2[\hat{S}_2\hat{S}_3 + \hat{S}_8\hat{S}_9] \\ &-J_3[\hat{S}_3\hat{S}_4 + \hat{S}_9\hat{S}_{10}] - J_4[\hat{S}_4\hat{S}_5 + \hat{S}_{10}\hat{S}_{11}] \\ &-J_5[\hat{S}_5\hat{S}_6 + \hat{S}_{11}\hat{S}_{12}] - J_6[\hat{S}_6\hat{S}_7 + \hat{S}_1\hat{S}_{12}] \qquad (2)\end{aligned}$$

The J values calculated using the whole molecule from the two available crystal structures are collected in Table 1, together with the values reported by Foguet-Albiol et al.,[32] who used simple dinuclear models to describe these interactions. For these calculations, we have used the seven low-lying spin configurations that provide a solvable system of

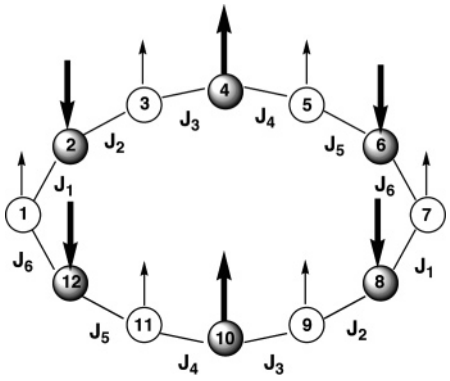

Figure 2. Scheme showing the topology of the exchange interactions in the studied Mn_{12} complex. The arrows indicate the most stable spin configuration that has a total spin $S = 7$ (thin arrows for $S = 2$ Mn^{III} cations; thick arrows for $S = 5/2$ Mn^{II} cations).

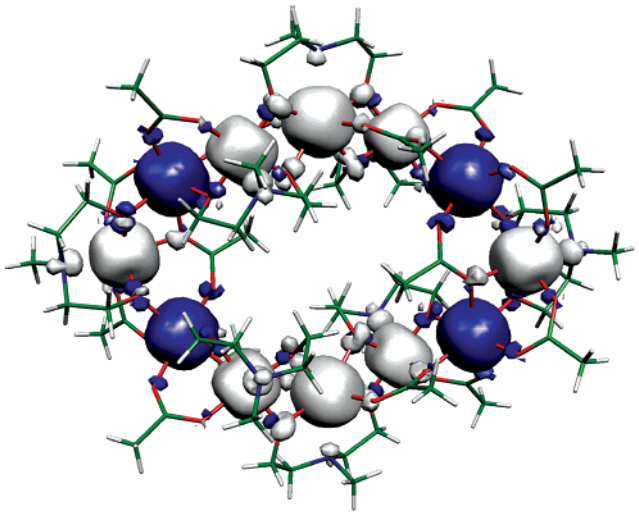

Figure 3. Spin density map for the $S = 7$ single-determinant ground state of the Mn_{12} loop complex, calculated with the B3LYP functional. The isodensity surface represented corresponds to a value of 0.005 e^-/bohr^3 (white and blue regions indicate positive and negative spin populations, respectively).

equations (see Computational Details section), that is, the minimum needed to obtain the six J values. The analysis of the results allows us to extract the following conclusions: (i) The J_1, J_2, and J_5 coupling constants correspond to similar sets of three bridging ligands and consequently present nearly the same weakly antiferromagnetic values. Interactions through a set of one carboxylato and one alkoxo bridges with an additional monodentate carboxylato bridging ligand with long Mn−O bond distances are known to be weakly antiferromagnetic.[33] (ii) The J_3 and J_4 exchange interactions occur through similar bridging ligands and are weakly ferromagnetic, essentially through the two alkoxo bridges since the carboxylato ligands have long bond distances to the metals, especially with the Mn^{III} cation due to the Jahn−Teller effect. (iii) The J_6 coupling constant calculated using the B3LYP functional also corresponds to a weak antiferromagnetic interaction, at difference with the negligible coupling constant obtained by Foguet-Albiol et al. with dinuclear models.[32] Only with one of the structures and the Perdew, Burke, and Erzernhof (PBE) functional do we obtain a very weak J_6 ferromagnetic interaction. We must note that an antiferromagnetic J_6 value is mandatory to obtain a single-determinant ground state with $S = 7$ as found experimentally, whereas an $S = 0$ ground state is predicted for a ferromagnetic J_6 coupling. Hence, our calculated values are consistent with the ground spin configuration with $S = 7$ shown in Figure 2, in agreement with the experimental ground state proposed by Foguet-Albiol et al.[32] It must be pointed out, however, that we have estimated energies of the states diagonalizing an approximate half-molecule model that shows the presence of an $S = 8$ state around 10 cm^{-1} above the ground state that could explain why the magnetic susceptibility can as well be fitted using an $S = 8$ ground state as proposed by Rumberger et al.[30,31]

The B3LYP calculated spin-density values (see Table 1) show a poor spin delocalization, as expected. The PBE functional gives a larger delocalization and, consequently, stronger interactions.[34,35] In Figure 3, we represent the spin density of the single determinant ground state that reveals

Table 1. Exchange Coupling Constants (in cm^{-1}) for the Mn_{12} Complex, $[Mn^{III}_6Mn^{II}_6(O_2CMe)_{14}(mda)_8]$, and Atomic Spin Populations (ρ) Calculated with the PBE (Siesta code) and B3LYP (Gaussian code) Functionals (see Computational Details Section) Using the Two Available Crystal Structures[30,32] [a]

	bridging ligands	Mn···Mn	Mn−X[b]	Mn−X−Mn	PBE	B3LYP[c]	B3LYP-m[d]
J_1	μ-O_2CMe, μ-OR μ-OCOMe	3.206	*2.120, 2.183, 2.250* 1.976, 1.901, 2.177	103.3, 92.8	−11.4(−6.0)	−4.1(−5.6)	−2.8
J_2	μ-O_2CMe, μ-OR μ-OCOMe	3.149	*2.097, 2.195, 2.159* 1.949, 1.916, 2.255	103.3, 90.1	−18.3(−14.9)	−8.0 (−2.5)	−9.2
J_3	μ-O_2CMe, 2 μ-OR	3.169	*2.245, 2.234, 2.210* 2.255, 1.907, 1.882	101.2, 99.6	+6.5 (+10.9)	+4.6 (+6.3)	+7.0
J_4	μ-O_2CMe, 2 μ-OR	3.183	*2.234, 2.204, 2.288* 2.198, 1.901, 1.889	101.4, 98.8	+6.6 (+9.2)	+4.6 (+5.4)	+8.0
J_5	μ-O_2CMe, μ-OR μ-OCOMe	3.198	*2.201, 2.172, 2.222* 1.984, 1.928, 2.198	102.3, 92.6	−8.4 (−5.4)	−2.8 (−5.9)	−5.0
J_6	2 μ-O_2CMe, μ-OR	3.473	*2.200, 2.143, 2.110* 1.989, 1.914, 2.177	117.6	−0.9 (+1.2)	−7.0 (−3.5)	+0.04
$\rho(Mn^{II})$					4.69	4.82	
$\rho(Mn^{III})$					3.80	3.85	

[a] Geometrical parameters of the structure published by Rumberger et al.[30,31] are also given (distances in Å, bond angles in degrees). [b] Values in italics correspond to the Mn^{II} cations. [c] In parentheses are those corresponding to the structure obtained by Foguet-Albiol at al. [d] Values obtained with dinuclear models (ref 18).

Table 2. Exchange Coupling Constants (in cm^{-1}) for $[Mn^{III}_6Mn^{II}_6(O_2CMe)_{14}(mda)_8]$[30,31] Calculated with the PBE and B3LYP Functionals Using Different Sets of *n* Spin Configurations[a]

	PBE				
n	6	13	16	24	32
J_1	−11.4	−10.8 (9)	−10.6 (9)	−10.4 (6)	−12.1 (7)
J_2	−18.3	−15.3 (8)	−15.4 (9)	−16.0 (5)	−16.3 (6)
J_3	+6.5	+6.6 (5)	+6.4 (5)	+6.5 (4)	+6.4 (5)
J_4	+6.6	+8.6 (7)	+8.5 (5)	+8.3 (3)	+8.1 (4)
J_5	−8.4	−7.2 (8)	−7.7 (7)	−8.2 (4)	−8.4 (5)
J_6	−0.9	−2.9 (10)	−1.8 (8)	−1.2 (4)	−1.8 (4)
	B3LYP				
n	6	13	16	24	32
J_1	−4.11	−3.9 (3)	−3.8 (3)	−3.8 (2)	−4.4 (3)
J_2	−7.96	−6.8 (3)	−6.9 (3)	−7.1 (1)	−7.2 (2)
J_3	+4.60	+4.6 (2)	+4.6 (2)	+4.6 (2)	+4.5 (2)
J_4	+4.61	+5.4 (2)	+5.3 (2)	+5.2 (1)	+5.1 (2)
J_5	−2.77	−2.3 (3)	−2.5 (3)	−2.7 (2)	−2.8 (2)
J_6	−7.03	−7.8 (4)	−7.3 (3)	−7.1 (2)	−7.3 (2)

[a] The number in parentheses indicates the standard deviation of the least-squares fitting.

the weak spin delocalization. The spin density at the Mn^{II} cations remains almost spherical. At the bridging ligand mediating ferromagnetic interactions (J_3 and J_4), spin polarization contributions show up in both positive and negative spin density lobes at the same atom.

Influence of the Choice of Spin Configurations on the Calculated *J* Values. In order to check the influence of the number of configurations employed in the calculations, we have analyzed the results taking up to 32 spin configurations together with the $S = 7$ ground-state spin solution. The fitted *J* values are collected in Table 2. In each case, the configurations correspond to the low-lying cases that provide a solvable system of equations. The analysis of the results gives some insights: (i) The nature and relative strength of the exchange interaction is well-reproduced by both functionals (PBE and B3LYP) independently of the number of spin configurations considered. (ii) The standard deviations are smaller than one wavenumber in all cases, independently of the magnitude of the interaction. (iii) The errors obtained with the PBE functional are slightly larger than those obtained with the hybrid functional. (iv) The inclusion of spin configurations with relatively high energies in the case of $n = 32$ induces rather small variations in the *J* values that are practically converged with a smaller number of spin configurations. (v) For the weakest interaction (J_6), the errors obtained with the PBE functional are approximately of the same order of magnitude as the coupling constant, although the sign remains unchanged for all numbers of spin configurations.

Role of the Next-Nearest Neighbor Interactions. As mentioned in the introduction, one of the goals of this work was to study the role of the next-nearest neighbor interactions. Due to the cyclic structure of the complex, it is a good test case to verify such an effect independently of other terms, such as the fourth-order terms that have also been proposed

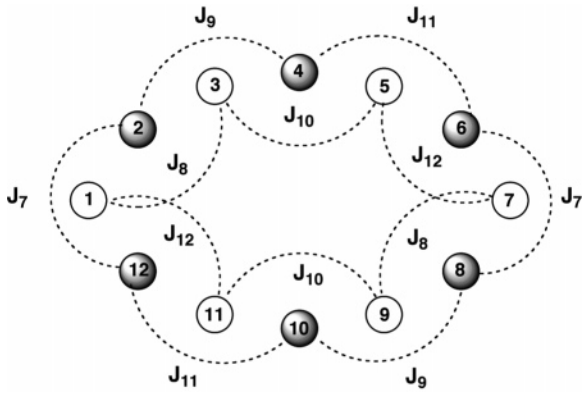

Figure 4. Scheme showing the topology of the next-nearest neighbor exchange interactions in the studied Mn_{12} complex.

to improve the description of the Hamiltonian. Such next-nearest neighbor interactions are depicted in Figure 4 with the corresponding mathematical expression for the Heisenberg Hamiltonian given in eq 3. With that Hamiltonian, J_1-J_6 are nearest-neighbor coupling constants and J_7-J_{12} correspond to next-nearest neighbor interactions.

$$\hat{H} = -J_1[\hat{S}_1\hat{S}_2 + \hat{S}_7\hat{S}_8] - J_2[\hat{S}_2\hat{S}_3 + \hat{S}_8\hat{S}_9] - J_3[\hat{S}_3\hat{S}_4 + \hat{S}_9\hat{S}_{10}] - J_4[\hat{S}_4\hat{S}_5 + \hat{S}_{10}\hat{S}_{11}] - J_5[\hat{S}_5\hat{S}_6 + \hat{S}_{11}\hat{S}_{12}] - J_6[\hat{S}_6\hat{S}_7 + \hat{S}_1\hat{S}_{12}] - J_7[\hat{S}_1\hat{S}_3 + \hat{S}_7\hat{S}_9] - J_8[\hat{S}_2\hat{S}_4 + \hat{S}_8\hat{S}_{10}] - J_9[\hat{S}_3\hat{S}_5 + \hat{S}_9\hat{S}_{11}] - J_{10}[\hat{S}_4\hat{S}_6 + \hat{S}_{10}\hat{S}_{12}] - J_{11}[\hat{S}_5\hat{S}_7 + \hat{S}_1\hat{S}_{11}] - J_{12}[\hat{S}_6\hat{S}_8 + \hat{S}_2\hat{S}_{12}] \quad (3)$$

The *J* values calculated including the next-nearest neighbor interactions with different sets of spin configurations are presented in Table 3. The main conclusions that can be extracted from such results are as follows: (i) The inclusion of the next-nearest neighbor interactions does not change significantly the magnitudes of the first neighbor coupling constants but reduces the error by around 1 order of magnitude, becoming smaller than 0.01 cm^{-1} in the case of the hybrid functional. Such results are reported with three decimals to show the accuracy reached in the fitting procedure even if it is probably beyond their physical accuracy. (ii) The convergence of the *J* values with the number of configurations is faster and smoother than when only first-neighbor interactions are considered. (iii) In the case of the PBE functional, the errors are larger than those obtained with the hybrid functional. (iv) The PBE functional gives a higher value of the J_6 coupling constants when next-nearest neighbor interactions are considered, becoming closer to the B3LYP results. (v) Only in the case of J_7 is the value of the next-nearest neighbor coupling constant significant, which should be attributed to the presence of a direct interaction through an anti-syn carboxylato bridging ligand[36] between the two metals (see Figure 1). (vi) All other next-nearest neighbor interactions show a very weak antiferromagnetic coupling with the exception of J_{12}, which is practically negligible.

Quantum Monte Carlo Simulations. In order to verify the applicability of the calculated *J* values, we wish to compare the experimental magnetic susceptibility curve with

Table 3. Exchange Coupling Constants (cm^{-1}) for $[Mn^{III}_6Mn^{II}_6(O_2CMe)_{14}(mda)_8]$[30,31] Including the Next-Nearest Neighbor Interactions (see Figures 2 and 4) Calculated with the PBE and B3LYP Functionals Using Different Sets of *n* Spin Configurations[a]

	PBE				
n	12	13	16	24	32
J_1	−12.00	−11.98 (10)	−11.96 (10)	−11.94 (8)	−11.95 (5)
J_2	−15.54	−15.50 (9)	−15.46 (9)	−15.51 (9)	−15.60 (5)
J_3	+5.87	+5.88 (8)	+5.88 (10)	+5.90 (9)	+5.83 (5)
J_4	+7.83	+7.80 (8)	+7.82 (9)	+7.94 (8)	+7.90 (5)
J_5	−7.37	−7.46 (10)	−7.37 (7)	−7.40 (7)	−7.34 (4)
J_6	−3.38	−3.28 (10)	−3.22 (8)	−3.21 (9)	−3.29 (4)
J_7	−1.96	−1.95 (7)	−1.90 (6)	−1.90 (6)	−1.94 (2)
J_8	−0.19	−0.05 (13)	−0.02 (11)	−0.02 (8)	−0.10 (5)
J_9	−0.72	−0.76 (6)	−0.74 (7)	−0.78 (6)	−0.77 (4)
J_{10}	−0.35	−0.43 (7)	−0.41 (8)	−0.49 (7)	−0.44 (4)
J_{11}	−0.79	−0.78 (5)	−0.77 (5)	−0.75 (5)	−0.77 (4)
J_{12}	+0.06	+0.06 (8)	+0.13 (5)	+0.16 (6)	+0.18 (4)
	B3LYP				
n	12	13	16	24	32
J_1	−4.321	−4.320 (4)	−4.319 (6)	−4.316 (9)	−4.313 (6)
J_2	−6.858	−6.856 (4)	−6.853 (6)	−6.856 (9)	−6.876 (7)
J_3	+4.283	+4.283 (4)	+4.283 (6)	+4.269 (9)	+4.288 (7)
J_4	+5.071	+5.069 (3)	+5.067 (5)	+5.062 (8)	+5.076 (7)
J_5	−2.425	−2.429 (5)	−2.436 (6)	−2.448 (7)	−2.456 (6)
J_6	−7.917	−7.913 (5)	−7.907 (6)	−7.910 (9)	−7.907 (5)
J_7	−0.710	−0.709 (3)	−0.709 (3)	−0.709 (6)	−0.707 (3)
J_8	−0.015	−0.009 (6)	−0.000 (7)	+0.006 (8)	−0.001 (7)
J_9	−0.340	−0.342 (3)	−0.345 (4)	−0.351 (7)	−0.336 (6)
J_{10}	−0.135	−0.139 (3)	−0.143 (4)	−0.136 (7)	−0.145 (6)
J_{11}	−0.277	−0.276 (2)	−0.274 (3)	−0.273 (5)	−0.267 (5)
J_{12}	+0.000	+0.000 (3)	−0.000 (5)	−0.007 (6)	−0.008 (6)

[a] The number in parentheses indicates the standard deviation of the least-squares fitting.

that obtained from those calculated parameters. Since the large size of the Hamiltonian matrix prevents the exact diagonalization or the use of the Lanczos algorithm[37] on the whole matrix, we have employed quantum Monte Carlo simulations (see Computational Details) using the calculated *J* values obtained with the two available crystal structures using only first-neighbor interactions and the largest set of spin configurations (see Table 2). There are two relatively similar experimental curves (see Figure 5) that were obtained by fitting an $S = 8$ ground state[30,31] (white squares) or an $S = 7$ value (white circles).[32] Our results are in good agreement with the experimental data (especially those obtained with the B3LYP functional) for the decay region below 150 K where the PBE functional gives a too fast drop due to the higher J_2 antiferromagnetic value. We have employed a $g = 2$ value for the quantum Monte Carlo simulations. However, using $g = 1.95$ close to the $g = 1.91$ obtained from the fitting by Rumberger et al.,[32] our simulation matches almost perfectly the experimental curve.

From the shape of the magnetic susceptibility curves, it is not easy to conclude which is the total spin of the ground state; however, the theoretical results clearly indicate the presence of an $S = 7$ single-determinant ground state with an $S = 9$ excited-state very close in energy.

Conclusions

The exchange coupling constants calculated using methods based on density functional theory provide an accurate description of the available experimental magnetic properties of the studied loop Mn_{12} complex. Thus, the calculated exchange coupling constants using the hybrid B3LYP functional for the two experimental crystal structures predict an $S = 7$ single-determinant ground state in good agreement with the $S = 7$ and 8 values proposed experimentally.

The use of numerical calculations with the PBE functional gives fair results in general, although the weakest exchange coupling constant (J_6) calculated for one of the crystal structures has a wrong positive sign. The use of quantum Monte Carlo simulations indicates that the calculated exchange coupling constants using the B3LYP functional and a Gaussian basis set reproduce nicely the experimental curve with a better agreement than the PBE functional combined with a numerical basis set.

We have also analyzed the effect of the choice of the spin configurations for the calculation of the exchange coupling constants showing that the values obtained are practically independent of the number of spin configurations employed. The calculated errors are similar for all the interactions independently of their value, and such errors are larger for the numerical PBE results than for the B3LYP method using Gaussian functions as a basis set. The inclusion of next-nearest neighbor interactions reduces the errors in the exchange coupling constants by about one order of magnitude, while the values corresponding to the first-neighbor coupling constants remain practically unchanged. The convergence of the calculated *J* values with the number of spin configurations is faster and smoother than when only first-neighbor interactions are considered. The next-nearest neighbor interactions correspond usually to very weak antiferromagnetic coupling with the exception of J_7, which corresponds to an interaction through a syn-anti carboxylato bridging ligand between the two metals.

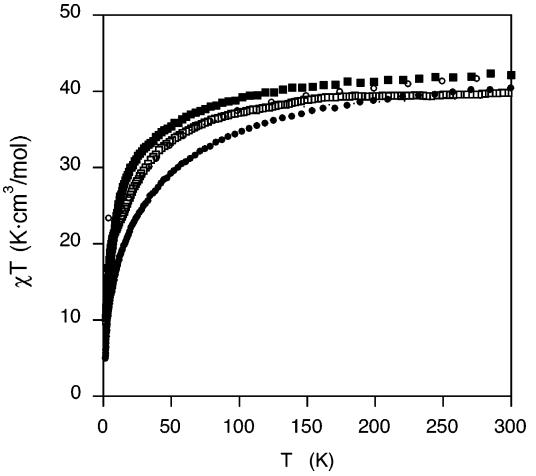

Figure 5. Temperature dependence of the magnetic susceptibility of the Mn_{12} complex, two experimental curves (white squares[30,31] and circles[32]), and from quantum Monte Carlo simulations using the coupling constants calculated with the PBE (black circles) and B3LYP (black squares) functionals (see Computational Details).

Computational Details

In our calculations, we have employed the experimental structures[32] due to the large dependence of the magnetic

Table 4. Spin Configurations Employed in the Calculations Sorted by Energy, with Exception of the First 12 Configurations That Were Selected to Have a Solvable System of Equations, with Their Total Spin Value[a]

	atoms with down spin	*S*		atoms with down spin	*S*
sd0	Mn2, Mn4, Mn8, Mn10	7	**sd17**	Mn2, Mn4, Mn7, Mn10	8
sd1	Mn2, Mn4, Mn9, Mn11	9	**sd18**	Mn1, Mn4, Mn7, Mn9, Mn11, Mn12	1
sd2	Mn2, Mn4, Mn7, Mn8, Mn10	3	**sd19**	Mn2, Mn3, Mn5, Mn6, Mn7, Mn10	0
sd3	Mn2, Mn4, Mn9, Mn11, Mn12	4	**sd20**	Mn4, Mn10	17
sd4	Mn2, Mn4, Mn7, Mn9, Mn10	4	**sd21**	Mn1, Mn2, Mn4, Mn7, Mn10	4
sd5	Mn2, Mn4, Mn6, Mn7, Mn9, Mn11	0	**sd22**	Mn3, Mn9	19
sd6	Mn2, Mn4, Mn10	12	**sd23**	Mn2, Mn8	17
sd7	Mn3, Mn5, Mn6, Mn7, Mn10	5	**sd24**	Mn2, Mn4, Mn7, Mn10, Mn12	3
sd8	Mn2, Mn4, Mn6, Mn8, Mn10	2	**sd25**	Mn1, Mn4, Mn6, Mn7, Mn10	4
sd9	Mn2, Mn4, Mn8	12	**sd26**	Mn2, Mn3, Mn5, Mn7, Mn10	5
sd10	Mn2, Mn4, Mn5, Mn8, Mn10	3	**sd27**	Mn1, Mn4, Mn7, Mn10	9
sd11	Mn2, Mn3, Mn4, Mn8, Mn10	3	**sd28**	Mn2, Mn3	18
sd12	Mn2, Mn4, Mn7, Mn9	9	**sd29**	Mn5, Mn11	19
sd13	Mn2, Mn4, Mn7, Mn9, Mn11	5	**sd30**	–	27
sd14	Mn2, Mn5, Mn6, Mn7, Mn10	4	**sd31**	Mn1, Mn7	19
sd15	Mn2, Mn4, Mn7, Mn9, Mn11, Mn12	0	**sd32**	Mn6, Mn12	17
sd16	Mn2, Mn3, Mn5, Mn8, Mn10	4			

[a] Mn^{III} and Mn^{II} cations correspond to odd and even numbers, respectively.

properties with structural parameters, and very small variations in the geometry such as those induced by packing forces can produce large changes in the calculated exchange coupling constants.[18,38] The calculations with the B3LYP functional[39] were performed with the NWChem code (version 4.7)[40,41] and a guess function generated with the Jaguar 6.0 code.[42] The triple-ζ all-electron Gaussian basis set proposed by Schaefer et al. was employed.[43] The NWChem calculations were carried out in parallel using 256 processors in a JS21 cluster at the Barcelona Supercomputer Center.

The SIESTA program (Spanish Initiative for Electronic Simulations with Thousands of Atoms)[44−47] was employed with the GGA exchange-correlation functional proposed by Perdew, Burke, and Erzernhof (PBE).[48] We have selected values of 50 meV for the energy shift and 200 Ry for mesh cutoff that provide a good compromise between accuracy and computer time needed to calculate the exchange coupling constants.[49,50] Only external electrons are included in the calculations, the cores being replaced by norm-conserving scalar relativistic pseudopotentials factorized in the Kleinman−Bylander form.[51] These pseudopotentials are generated following the approach proposed by Trouiller and Martins[52] from the ground-state atomic configurations for all the atoms except for Mn, for which the Mn^{II} configuration $[Ne]3s^2-3p^64s^03d^5$ was employed. The core radii for the s, p, and d components of the Mn atoms are 1.4, 1.9, and 1.5, respectively, and we have included partial-core corrections for a better description of the core regions.[53] The cutoff radii were 1.15 for oxygen, nitrogen, and hydrogen atoms; 1.25 for carbon; and 1.6 for chlorine atoms.

The spin configurations adopted for the $[Mn^{III}_6Mn^{II}_6(O_2CMe)_{14}(mda)_8]$ complex in order to obtain the exchange coupling constants are collected in Table 4.

Due to the impossibility to perform the exact diagonalization of the Hamiltonian matrix because of its huge size, we have employed quantum Monte Carlo simulations that allow the treatment of quantum spin systems.[54] Among them, we have employed the decoupled cell Monte Carlo method proposed by Homma et al.[55,56] The basic idea of such simulations is to perform the exact diagonalization only for a small subsystem, the decoupled cell. The conditional probability of a spin placed in the center of the subsystem being up or down is obtained from these exact diagonalization procedures, then it is possible to construct a Markov chain of a quantum system by using the Metropolis algorithm as in the classical Monte Carlo approach. In this case, we have employed a cell considering five atoms including, in such a way, the interactions of the central atom with first and next-nearest neighbors. In general, the quality of such quantum methods will depend on the size of the cell employed in the calculation of the probabilities, being hypothetically exact when the whole system is considered. We have employed successfully these kinds of simulations previously in single-molecule magnets, for instance, in an Fe_8 complex.[57] The simulations reproduce correctly the results of the exact diagonalization of the Hamiltonian down to relatively low temperatures.

Acknowledgment. The research reported here was supported by the Dirección General de Investigación del Ministerio de Educación y Ciencia and Comissió Interdepartamental de Ciència i Tecnologia (CIRIT) through grants CTQ2005-08123-C02-02/BQU and 2005SGR-00036, respectively. The authors thankfully acknowledge the computer resources, technical expertise, and assistance provided by the Barcelona Supercomputing Center (Centro Nacional de Supercomputación). R.C. thanks the Ministerio de Educación y Ciencia for a Mobility Program grant to cover his stay in Barcelona.

References

(1) Miller, J. S.; Drillon, M. *Magnetism: Molecules to Materials*; Wiley-VCH: Weinheim, Germany, 2001−2005; Vol. 1−5.
(2) Aromí, G.; Brechin, E. *Struct. Bonding* **2006**, *122*, 1.
(3) Christou, G. *Polyhedron* **2005**, *24*, 2065.
(4) Caneschi, A.; Gatteschi, D.; Sessoli, R.; Barra, A. L.; Brunel, L. C.; Guillot, M. *J. Am. Chem. Soc.* **1991**, *113*, 5873.
(5) Friedman, J. R.; Sarachik, M. P.; Tejada, J.; Ziolo, R. *Phys. Rev. Lett.* **1996**, *76*, 3830.
(6) Thomas, L.; Lionti, F.; Ballou, R.; Sessoli, R.; Gatteschi, D.; Barbara, B. *Nature (London, U.K.)* **1996**, *383*, 145.
(7) Sessoli, R.; Gatteschi, D. *Angew. Chem., Int. Ed.* **2003**, *42*, 246.
(8) Gatteschi, D.; Sessoli, R.; Villain, J. *Molecular Nanomagnets*; Oxford University Press: Oxford, U. K., 2006.

(9) Pederson, M. R.; Khanna, S. N. *Phys. Rev. B: Condens. Matter Mater. Phys.* **1999**, *60*, 9566.

(10) Kortus, J.; Pederson, M. R.; Baruah, T.; Bernstein, N.; Hellberg, C. S. *Polyhedron* **2003**, *22*, 1871.

(11) Pederson, M. R.; Bernstein, N.; Kortus, J. *Phys. Rev. Lett.* **2002**, *89*, 097202/1.

(12) Pederson, M. R.; Porezag, D. V.; Kortus, J.; Khanna, S. N. *J. Appl. Phys.* **2000**, *87*, 5487.

(13) Ruiz, E. *Struct. Bonding* **2004**, *113*, 71.

(14) Gatteschi, D. *J. Phys. Chem. B* **2001**, *104*, 9780.

(15) Goursot, A.; Malrieu, J. P.; Salahub, D. R. *Theor. Chim. Acta* **1995**, *91*, 225.

(16) Castro, M.; Salahub, D. R. *Phys. Rev. B: Condens. Matter Mater. Phys.* **1993**, *47*, 10955.

(17) Postnikov, A. V.; Kortus, J.; Pederson, M. R. *Phys. Status Solidi B* **2006**, *243*, 2533.

(18) Ruiz, E.; Alemany, P.; Alvarez, S.; Cano, J. *J. Am. Chem. Soc.* **1997**, *119*, 1297.

(19) Ruiz, E.; Alvarez, S.; Rodríguez-Fortea, A.; Alemany, P.; Pouillon, Y.; Massobrio, C. Electronic Structure and Magnetic Behavior in Polynuclear Transition-Metal Compounds. In *Magnetism: Molecules to Materials*; Miller, J. S., Drillon, M., Eds.; Wiley-VCH: Weinheim, Germany, 2001; Vol. 2, pp 227−279.

(20) Ruiz, E.; Cano, J.; Alvarez, S.; Caneschi, A.; Gatteschi, D. *J. Am. Chem. Soc.* **2003**, *125*, 6791.

(21) Boukhvalov, D. W.; Al-Saqer, M.; Kurmaev, E. Z.; Moewes, A.; Galakhov, V. R.; Finkelstein, L. D.; Chiuzbaian, S.; Neumann, M.; Dobrovitski, V. V.; Katsnelson, M. I.; Lichtenstein, A. I.; Harmon, B. N.; Endo, K.; North, J. M.; Dalal, N. S. *Phys. Rev. B: Condens. Matter Mater. Phys.* **2007**, *75*, 014419.

(22) Boukhvalov, D. W.; Lichtenstein, A. I.; Dobrovitski, V. V.; Katsnelson, M. I.; Harmon, B. N.; Mazurenko, V. V.; Anisimov, V. I. *Phys. Rev. B: Condens. Matter Mater. Phys.* **2002**, *65*, 184435.

(23) Park, K.; Pederson, M. R. *Phys. Rev. B: Condens. Matter Mater. Phys.* **2004**, *70*, 054414.

(24) Park, K.; Pederson, M. R.; Hellberg, C. S. *Phys. Rev. B: Condens. Matter Mater. Phys.* **2004**, *69*, 014416.

(25) Ruiz, E.; Cano, J.; Alvarez, S.; Alemany, P. *J. Comput. Chem.* **1999**, *20*, 1391.

(26) Ruiz, E.; Rodríguez-Fortea, A.; Cano, J.; Alvarez, S.; Alemany, P. *J. Comput. Chem.* **2003**, *24*, 982.

(27) Ruiz, E.; Alvarez, S.; Cano, J.; Polo, V. *J. Chem. Phys.* **2005**, *123*, 164110.

(28) Bencini, A.; Totti, F. *Int. J. Quantum Chem.* **2005**, *101*, 819.

(29) Moreira, I. d. P. R.; Calzado, C. J.; Malrieu, J. P.; Illas, F. *Phys. Rev. Lett.* **2006**, *97*, 087003.

(30) Rumberger, E. M.; Zakharov, L. N.; Rheingold, A. L.; Hendrickson, D. N. *Inorg. Chem.* **2004**, *43*, 6531.

(31) Rumberger, E. M.; Zakharov, L. N.; Rheingold, A. L.; Hendrickson, D. N. *Inorg. Chem.* **2005**, *44*, 2742.

(32) Foguet-Albiol, D.; O'Brien, T. A.; Wernsdorfer, W.; Moulton, B.; Zaworotko, M. J.; Abboud, K. A.; Christou, G. *Angew. Chem., Int. Ed.* **2005**, *44*, 897.

(33) Que, L.; True, A. E. *Prog. Inorg. Chem.* **1990**, *38*, 97.

(34) Cano, J.; Ruiz, E.; Alvarez, S.; Verdaguer, M. *Comments Inorg. Chem.* **1998**, *20*, 27.

(35) Ruiz, E.; Cirera, J.; Alvarez, S. *Coord. Chem. Rev.* **2005**, *249*, 2649.

(36) Rodriguez-Fortea, A.; Alemany, P.; Alvarez, S.; Ruiz, E. *Chem.—Eur. J.* **2001**, *7*, 627.

(37) Rajaraman, G.; Ruiz, E.; Cano, J.; Alvarez, S. *Chem. Phys. Lett.* **2005**, *415*, 6.

(38) Ruiz, E.; Cano, J.; Alvarez, S.; Alemany, P. *J. Am. Chem. Soc.* **1998**, *120*, 11122.

(39) Becke, A. D. *J. Chem. Phys.* **1993**, *98*, 5648.

(40) Kendall, R. A.; Apra, E.; Bernholdt, D. E.; Bylaska, E. J.; Dupuis, M.; Fann, G. I.; Harrison, R. J.; Ju, J. L.; Nichols, J. A.; Nieplocha, J.; Straatsma, T. P.; Windus, T. L.; Wong, A. T. *Comput. Phys. Commun.* **2000**, *128*, 260.

(41) Aprà, E.; Windus, T. L.; Straatsma, T. P.; Bylaska, E. J.; de Jong, W.; Hirata, S.; Valiev, M.; Hackler, M.; Pollack, L.; Kowalski, K.; Harrison, R.; Dupuis, M.; Smith, D. M. A.; Nieplocha, J. V. T.; Krishnan, M.; Auer, A. A.; Brown, E.; Cisneros, G.; Fann, G.; Fruchtl, H.; Garza, J.; Hirao, K.; Kendall, R.; Nichols, J.; Tsemekhman, K.; Wolinski, K.; Anchell, J.; Bernholdt, D.; Borowski, P.; Clark, T.; Clerc, D.; Dachsel, H.; Deegan, M.; Dyall, K.; Elwood, D.; Glendening, E.; Gutowski, M.; Hess, A.; Jaffe, J.; Johnson, B.; Ju, J.; Kobayashi, R.; Kutteh, R.; Lin, Z.; Littlefield, R.; Long, X.; Meng, B.; Nakajima, T.; Niu, S.; Rosing, M.; Sandrone, G.; Stave, M.; Taylor, H.; Thomas, G.; van Lenthe, J.; Wong, A.; Zhang, Z. *NWChem, A Computational Chemistry Package for Parallel Computers*, Version 4.7; Pacific Northwest National Laboratory: Richland, WA, 2005.

(42) *Jaguar 6.0*; Schrödinger, Inc.: Portland, OR, 2005.

(43) Schaefer, A.; Huber, C.; Ahlrichs, R. *J. Chem. Phys.* **1994**, *100*, 5829.

(44) Artacho, E.; Gale, J. D.; García, A.; Junquera, J.; Martin, R. M.; Ordejón, P.; Sánchez-Portal, D.; Soler, J. M. *SIESTA*, v.1.3; Siesta: Madrid, Spain, 2001.

(45) Soler, J. M.; Artacho, E.; Gale, J. D.; García, A.; Junquera, J.; Ordejón, P.; Sánchez-Portal, D. *J. Phys.: Condens. Matter* **2002**, *14*, 2745.

(46) Artacho, E.; Sánchez-Portal, D.; Ordejón, P.; García, A.; Soler, J. M. *Phys. Status Solidi A* **1999**, *215*, 809.

(47) Sánchez-Portal, D.; Ordejón, P.; Artacho, E.; Soler, J. M. *Int. J. Quantum Chem.* **1997**, *65*, 453.

(48) Perdew, J.; Burke, K.; Ernzerhof, M. *Phys. Rev. Lett.* **1996**, *77*, 3865.

(49) Massobrio, C.; Ruiz, E. *Monatsh. Chem.* **2003**, *134*, 317.

(50) Ruiz, E.; Rodríguez-Fortea, A.; Tercero, J.; Cauchy, T.; Massobrio, C. *J. Chem. Phys.* **2005**, *123*, 074102.

(51) Kleinman, L.; Bylander, D. M. *Phys. Rev. Lett.* **1982**, *48*, 1425.

(52) Trouiller, N.; Martins, J. L. *Phys. Rev. B: Condens. Matter Mater. Phys.* **1991**, *43*, 1993.

(53) Louie, S. G.; Froyen, S.; Cohen, M. L. *Phys. Rev. B: Condens. Matter Mater. Phys.* **1982**, *26*, 1982.

(54) Suzuki, M. *Quantum Monte Carlo Methods*; Springer-Verlag: Berlin 1987; Springer Series in Solid-State Science Vol. 74.

(55) Homma, S.; Matsuda, H.; Ogita, N. *Prog. Theor. Phys.* **1986**, *75*, 1058.

(56) Homma, S. The Decoupled Cell Method of Quantum Monte Carlo Calculation. In *Quantum Monte Carlo Methods in Condensed Matter Physics*; Suzuki, M., Ed.; World Scientific Publishing Co. Pte. Ltd.: Singapore, 1993; pp 163−177.

(57) Ruiz, E.; Cano, J.; Alvarez, S. *Chem.—Eur. J.* **2005**, *11*, 4767.

CT700013G